

ORIGINAL ARTICLE

Early Development of Functional Network Segregation Revealed by Connectomic Analysis of the Preterm Human Brain

Miao Cao¹, Yong He¹, Zhengjia Dai¹, Xuhong Liao¹, Tina Jeon², Minhui Ouyang², Lina Chalak³, Yanchao Bi¹, Nancy Rollins⁴, Qi Dong¹ and Hao Huang^{2,5}

¹State Key Laboratory of Cognitive Neuroscience and Learning and IDG/McGovern Institute for Brain Research, Beijing Normal University, Beijing 100875, China, ²Department of Radiology, Children's Hospital of Philadelphia, Philadelphia, PA 19104, USA, ³Department of Pediatrics and, ⁴Department of Radiology, University of Texas Southwestern Medical Center, Dallas, TX 75390, USA and ⁵Department of Radiology, University of Pennsylvania, Philadelphia, PA 19104, USA

Address correspondence to Yong He, State Key Laboratory of Cognitive Neuroscience and Learning and IDG/McGovern Institute for Brain Research, Beijing Normal University, Beijing, 100875, China. Email: yong.he@bnu.edu.cn; Hao Huang, Department of Radiology, University of Pennsylvania, Philadelphia, PA 19104, USA. Email: huangh6@email.chop.edu

Abstract

Human brain functional networks are topologically organized with nontrivial connectivity characteristics such as small-worldness and densely linked hubs to support highly segregated and integrated information processing. However, how they emerge and change at very early developmental phases remains poorly understood. Here, we used resting-state functional MRI and voxel-based graph theory analysis to systematically investigate the topological organization of whole-brain networks in 40 infants aged around 31 to 42 postmenstrual weeks. The functional connectivity strength and heterogeneity increased significantly in primary motor, somatosensory, visual, and auditory regions, but much less in high-order default-mode and executive-control regions. The hub and rich-club structures in primary regions were already present at around 31 postmenstrual weeks and exhibited remarkable expansions with age, accompanied by increased local clustering and shortest path length, indicating a transition from a relatively random to a more organized configuration. Moreover, multivariate pattern analysis using support vector regression revealed that individual brain maturity of preterm babies could be predicted by the network connectivity patterns. Collectively, we highlighted a gradually enhanced functional network segregation manner in the third trimester, which is primarily driven by the rapid increases of functional connectivity of the primary regions, providing crucial insights into the topological development patterns prior to birth.

Key words: connectome, functional connectivity, hub, preterm, rich club

Introduction

The topological principles of human brain networks have recently been extensively studied with noninvasive neuroimaging methods. The spontaneous low-frequency fluctuations in brain

activities, monitored by blood oxygen level-dependent (BOLD) signals using resting-state functional magnetic resonance imaging (R-fMRI), have been found temporally correlated across functionally related areas (Friston 1994; Biswal et al.

1995). These correlations, referred to as functional connectivity, yield detailed maps of coordination across brain regions, comprising the “functional connectome” of individuals (Sporns et al. 2005; Biswal et al. 2010; Kelly et al. 2012). Employing the graph theory-based analysis method, several nontrivial topological properties have been discovered in the functional connectomes of healthy adults: small-worldness, which reflects an optimal balance between segregation and integration in information processing between regions (Salvador et al. 2005; Achard et al. 2006); the presence of a small number of hubs in the medial and lateral frontal and parietal cortices with disproportionately numerous connections (Buckner et al. 2009; Tomasi and Volkow 2011; Liang et al. 2013; van den Heuvel and Sporns 2013), which tend to be densely connected to each other, forming a “rich club” (van den Heuvel and Sporns 2011; van den Heuvel et al. 2012; Cao et al. 2014). Intriguingly, these key aspects of the functional connectome have been revealed to change significantly across development (Bullmore and Sporns 2009, 2012; Di Martino et al. 2014), raising the question of how they emerge and change at very early stages of human life.

In the brains of term babies, previous R-fMRI studies employing seed-based connectivity or independent component analyses have identified specific functional networks, including primary visual, auditory, and sensorimotor networks (Fransson et al. 2007, 2009; Doria et al. 2010; Smyser et al. 2010), and default-mode and executive-control networks involved in heteromodal functions (Doria et al. 2010; Smyser et al. 2010). Network analyses based on graph theory further revealed that the functional connectomes of infant brains already exhibited the small-world structure. Distinct from the adults, however, the hubs were largely confined to primary sensorimotor regions at term (Fransson et al. 2011; Gao et al. 2011). Studying brains even younger than full-term birth is crucial to understand how these topological properties appeared.

Prior to the normal time of birth, rapid neuronal growth occurs during the third trimester of pregnancy. Neurons migrating from ventricular and subventricular zone along the radial glial scaffold (Rakic 1972, 1995; Sidman and Rakic 1973) interact with each other as well as neurons in the cortical plate through synaptic formation, dendritic arborization, and axonal growth (Molliver et al. 1973; Kostovic and Jovanov-Milosevic 2006; Bystron et al. 2008). The interconnected neurons are thought to have resulted in the formation and differentiation of significant functional circuits, fostering emergence of primary sensorimotor functions and higher cognitive skills (Dehaene-Lambertz and Spelke 2015). Using R-fMRI data obtained from fetuses or premature infants, developmental curves of various specific functional connections have been depicted (Doria et al. 2010; Smyser et al. 2010; Jakab et al. 2014; Thomason et al. 2015; Toulmin et al. 2015; Ball et al. 2016). However, it remains largely unknown about the emergence and maturation process of the large-scale topological properties of the functional connectomes, such as the functional segregation and integration patterns, at this critical developmental stage.

Here, we employed R-fMRI and voxel-based graph theory analysis approaches to investigate topological properties of whole-brain functional networks in 40 term and preterm infants postmenstrual aged 31.3–41.7 weeks at the scan time. We first assessed the spatiotemporal dynamics of functional connectivity by measuring correlation of spontaneous BOLD signals among every pair of brain voxels in the whole brain and examining these changes along anatomical distances for each infant. Subsequently, we explored the emergence and age-dependent changes of the topological properties of functional brain connectome,

including small-worldness, modular structure, hubs, and rich clubs. We hypothesized that 1) this period is marked by a gradual transition from a relatively random to a more organized network, characterized by increased functional connectivity and local network clustering, and 2) such topological changes are primarily driven by the disproportionate growth of the primary functional systems in preparation for the basic survival functions at birth.

Materials and Methods

Participants

We recruited 52 normal preterm and term infants with postmenstrual age from 31.3 to 41.7 weeks at the scan time. Here, postmenstrual age was defined according to Engle’s descriptions (Engle 2004). The infants were part of the normal cohort for participating the research of studying normal brain maturation in this key neural developmental period and were not clinically indicated. The detailed demographic information is presented in Table 1. Briefly, all the infants were recruited from Parkland Hospital at Dallas and underwent an R-fMRI scan. These infants were selected through rigorous screening procedures by a board-certified neonatologist (L.C.). The exclusion criteria include the mother’s excessive drug or alcohol abuse during pregnancy; Grade III–IV intraventricular hemorrhage; periventricular leukomalacia; hypoxic–ischemic encephalopathy; body or heart malformations; chromosomal abnormalities, lung disease or bronchopulmonary dysplasia; necrotizing enterocolitis requiring resection or complex feeding/nutritional disorders; defects or anomalies of the forebrain, brainstem or cerebellum; brain tissue dysplasia or hypoplasia; abnormal meninges; alterations in the pial or ventricular surface; or white matter lesions. A pediatric radiologist (N.R.) with 25 years of experience confirmed no structural or signal abnormality with a dulcet image pattern appropriate for postmenstrual age after reading the MRI scans. Written and informed consent was obtained from the parents. This study was approved through the Institutional Review Board. After discarding the subjects with head motions exceeding thresholds (see “Image Preprocessing”), the R-fMRI data of 40 normal preterm and term infants were used for the data analysis.

Data Acquisition

The MRI data were acquired at a Philips 3T Achieva MR scanner with 8-channel SENSE head coil at the Children’s Medical Center at Dallas. The infants were well-fed prior to scanning. All MR scans were performed during natural sleep without sedation. A T_2 -weighted gradient-echo EPI sequence was used to obtain the R-fMRI scan. A total of 210 whole brain EPI volumes were acquired using the following parameters: TR = 1500 ms, TE = 27 ms, flip angle = 80°, in-plane imaging resolution = $2.4 \times 2.4 \text{ mm}^2$, in-plane field of view (FOV) = $168 \times 168 \text{ mm}^2$, slice thickness = 3 mm, with no gap; slice number = 30. The R-fMRI scan time was 5.4 min. A co-registered T_2 -weighted image was acquired with turbo spin echo (TSE) sequence as the structural MRI with the following parameters: TR = 3000 ms, effective TE = 80 ms, in-plane imaging resolution = $1.5 \times 1.5 \text{ mm}^2$, in-plane field of view (FOV) = $168 \times 168 \text{ mm}^2$, slice thickness = 1.6 mm with no gap, slice number = 65. The acquired T_2 -weighted image was zero-filled to 256×256 image matrix.

Data Analysis

Image Preprocessing

The BOLD fMRI images were preprocessed using Statistical Parametric Mapping (SPM8, <http://www.fil.ion.ucl.ac.uk/spm>) and

Table 1 Demographic information for the preterm and term infants

	Number of infants	Age range (weeks)	Age mean (weeks)	Weight range (kg)	Weight mean (kg)	Male, n (%)	White, n (%)	Mode of delivery ^a	Feeding practice ^b	Antibiotic exposure during pregnancy
Infants scanned during R-fMRI										
At birth	52	25.1–41.0	33.4	0.8–4.0	2.2	37 (71)	38 (73)	C: 30; V: 22	B: 52; F: 0	Yes
At scan	52	31.3–41.7	36.4	1.4–4.1	2.5	37 (71)	38 (73)	C: 30; V: 22	B: 52; F: 0	Yes
Infants with acceptable h/m during R-fMRI										
At birth	40	25.1–40.7	33.2	0.8–4.0	2.1	29 (73)	30 (75)	C: 24; V: 16	B: 40; F: 0	Yes
At scan	40	31.3–41.7	37.0	1.4–4.1	2.6	29 (73)	30 (75)	C: 24; V: 16	B: 40; F: 0	Yes

Note: The acceptable head motion (h/m) includes translation <5 mm, rotation <5°, and mFD <1 mm.

^aC for C-section and V for vaginal birth.

^bB for breast-feeding and F for formula.

Data Processing Assistant for Resting-State fMRI [DPARSF, (Yan and Zang 2010)]. Before the preprocessing, we removed the first 15 volumes for signal to reach a steady state, leaving 195 functional volumes for each subject. These functional data were then corrected for acquisition time delay between slices and head motion between volumes. The data of 12 subjects were discarded from further analysis, due to their head motion displacements >5 mm, rotation >5°, or mean frame-wise displacement (mFD) >1 mm (Power et al. 2012). Within the remaining 40 subjects, the head motion parameters showed no significant correlation with age (mFD: $r = 0.03$, $P = 0.831$). The head motion corrected functional data were subject to the following imaging process. Briefly, these functional data were first aligned with their corresponding high-resolution T_2 -weighted structural images using a linear transformation. Then, the individual T_2 -weighted images were nonlinearly registered to a 37-week brain template (Serag et al. 2012). A customized template was generated through averaging the resultant normalized T_2 -weighted structural images of all subjects. Individual T_2 -weighted images were further nonlinearly registered to the custom template. The aligned functional data were normalized by applying the transformation parameters estimated during the second registration of T_2 -weighted images and resampled to 3 mm isotropic voxels. The template of the cortex, deep gray matter, white matter, and cerebrospinal fluid tissue templates at 37 weeks were also registered to the customized template for following mask generation (Serag et al. 2012). The normalized functional images further underwent spatially smoothing with a Gaussian kernel (full width at half-maximum of 4 mm), linear trend removal, and temporal band-pass filtering (0.01–0.10 Hz). Finally, several nuisance variables, including Friston's 24 head motion parameters (Friston et al. 1996), the averaged signal from white matter and cerebrospinal fluid tissue, were removed through multiple linear regression analysis to reduce the effects of nonneuronal signals.

Functional Correlation Matrix Formation

In this study, we constructed the functional correlation matrices at a voxel level. A gray matter mask (number of voxels = 7101) was predefined through thresholding the combing cortex and deep gray matter probability templates. Pearson's correlation between the BOLD time series of each pair of voxels within the gray matter mask was calculated. Fisher's r -to- z transformation was applied to improve the normality of the correlation coefficients, and the

absolute values of all correlations were used to obtain the correlation matrix for each subject. Notably, connectivity terminating within 10 mm of each source voxel center was set to zero to avoid potential shared signals between nearby voxels.

Functional Connectivity Analysis

To explore age effects on functional connectivity, we calculated the voxel-wise functional connectivity strength (FCS) values. Specifically, for each voxel, the FCS was calculated as the average of the correlations between this voxel and all other voxels in the brain. The mean strength and the heterogeneity of FCS were calculated for global description. Here, FCS heterogeneity was defined as $H = \Delta / \langle \text{FCS} \rangle$, where $\Delta = \sum_i \sum_j |\text{FCS}_i - \text{FCS}_j| / (n \times (n - 1))$ is the average absolute FCS differences of all pairs of nodes (i and j), and n is the number of nodes ($n = 7101$). To examine the developmental effects on nodal FCS, a general linear model (GLM) analysis was then performed in a voxel-wise manner. Multiple comparisons were performed using Monte Carlo simulations (For details, see the following "Statistical Analysis" section).

To further explore the distance effects on age-related connectivity changes, FCS was calculated at different distance bins. Specifically, we calculated the Euclidean distance, D_{ij} , as an approximate anatomical distance of functional connectivity between voxel i and voxel j and then divided whole brain functional connectivity maps into 5 bins with Euclidean distances binned into 20 mm steps, ranging from 10 to 110 mm (i.e., the longest distance between voxels in the gray matter mask). For every voxel, the FCS at each bin was calculated. Voxel-wise GLM analysis was conducted again to explore the age effects on distance-dependent FCS. Notably, considering the FCS maps in different distance bins contained different numbers of gray matter voxels, we performed the multiple comparison corrections within the respective masks (size range: 41 148–191 727 mm³).

Besides, a complimentary seed-based functional connectivity analysis was also conducted to explore detailed information of the connectional changes. We defined 6 seed regions of interest (ROIs) as 5 mm radius spheres centered on the maximal peak voxels of regional clusters showing significant age-related changes on FCS. The ROIs included the right thalamus, left lingual gyrus, left precentral gyrus, posterior cingulate/precuneus cortex (PCC/PCu), and bilateral rolandic operculum. For each seed ROI, we performed individual functional connectivity analysis by correlating the mean time series of the seed ROI with

those of all voxels within the gray matter mask. A Fisher's r -to- z transformation was further applied to improve the normality of the resulting correlation coefficient. We divided all the subjects into 3 groups according to their ages (Group 1: 31.3–35.3 weeks [$n = 14$]; Group 2: 35.6–38.4 weeks [$n = 12$]; and Group 3: 38.7–41.7 weeks [$n = 14$]). The seed-based functional connectivity patterns of each group were calculated using the 1-sample T -test. The term individuals were selected as the controls, and correlation patterns of them were also examined. Then we calculated the age-related changes on the functional connectivity with voxel-wise GLM analysis.

Functional Network Analysis

Functional brain networks were constructed by thresholding the correlation matrices with a density of 5%. The main network analyses were based on binarized brain networks. The effects of other connectivity densities and weighted network analysis on our results were also evaluated (see the following "Validation Analysis"). Notably, these voxel-wise brain network analyses were performed using our CPU-GUI platform (Wang et al. 2013). The following characteristic graph metrics were estimated to describe the topological organization development of the neonatal functional connectome.

Specifically, 1) to explore the age effects on global topological properties of whole brain functional networks, we computed small-world measures, including the clustering coefficient (C_p), the characteristic path length (L_p), their normalized versions (Γ and λ , respectively), and the small-worldness (Σ) (Watts and Strogatz 1998; Humphries et al. 2005). Notably, a network is said to be "small-world" when $\Sigma > 1$, which has both high global and local information transformation capacity (Watts and Strogatz 1998; Latora and Marchiori 2001; Humphries et al. 2005; Achard et al. 2006). Here, we used 100 corresponding random networks that were simultaneously matched in the distribution of correlation values and the connection density (5%) for each individual's practical network. This kind of random networks was considered the appropriate null models for correlation-based networks (Zalesky et al. 2012). 2) Furthermore, we explored the modular structure (i.e., sets of nodes that are highly interconnected but with relatively fewer connections to the others in different modules) in the brain networks and examined the changes in both modularity (Q) and modular number with age (Newman 2006). Louvain algorithm, which is a fast and accurate community detection algorithm for large networks (Blondel et al. 2008), was applied to individual brain network for modular analysis. 3) To explore age-related changes in nodal properties, we used nodal degree centrality, which indicates the number of connections linking a node with all other nodes. Nodes with high degree ($>$ mean + 1.5 SD) were identified as functional hubs, representing that they exhibit high connectivity to the rest of the brain. We further examined the node degree distribution for each subject. Moreover, nodal topological properties, including nodal efficiency, nodal clustering coefficient, and participation coefficient, were also computed (Watts and Strogatz 1998; Latora and Marchiori 2001; Newman 2006; Achard and Bullmore 2007). 4) Finally, to explore the core architectural changes, we identified the rich-club structure of brain functional networks, which is formed by the densely interconnected hubs (van den Heuvel and Sporns 2011; van den Heuvel et al. 2012; Cao et al. 2014), and further examined the changes in this structure over the age range. Detailed analyses of network properties are described in [Supplementary Materials and Methods](#).

Statistical Analysis

To detect developmental changes in both nodal and global properties, we used the following GLM, which included gender and mFD as covariates.

$$Y = \beta_0 + \beta_1 \times \text{age} + \beta_2 \times \text{gender} + \beta_3 \times mFD$$

Without other statements, the voxel-wise analyses were corrected for multiple comparisons and set to a corrected $P < 0.05$ (which corresponded to an uncorrected single voxel significance level of $P < 0.05$ and a minimum cluster size of 918 mm^3). This correction was confined within the gray matter mask (size: $191\,727 \text{ mm}^3$) and performed with Monte Carlo simulations (Ledberg et al. 1998) using the AFNI AlphaSim program (<http://afni.nimh.nih.gov/pub/dist/doc/manual/AlphaSim.pdf>).

Support Vector Regression Prediction Analysis

To determine whether the functional connectomic measurements could serve as biomarker for the brain maturity prediction, we performed multivariate pattern analysis using support vector regression approach. Chronological age was used as the training measure. Nodal FCS and whole-brain network metrics (including C_p , L_p , Σ , Q , rich-club coefficient, and rich club size) were used as features for the support vector regression predictor. We performed the prediction using a linear kernel function and the default settings of C51 with epsilon 50.001 in the LIBSVM Toolbox (<http://www.csie.ntu.edu.tw/~cjlin/libsvm/>) (Dosenbach et al. 2010). Leave-one-out cross-validation was used to evaluate the performance of support vector regression model. During each leave-one-out cross-validation iteration, we used the decision function derived from the training subjects to predict the brain age of the test subject. Pearson correlation coefficient between the actual and predicted ages was calculated to assess the prediction accuracy. The statistical significance of this prediction was assessed by permutation test. Specifically, for each prediction model, the age labels were randomly permuting 10 000 times. In each time, we calculated the Pearson correlation coefficient and used the empirical distribution to determine whether the observed correlation values could occur by change with 1-tailed test.

Procedures for Reducing Head Motion Artifact

To moderate the effects of head motion on estimates of functional connectivity and network metrics, we regressed out Friston's 24 head motion parameters in the preprocessing steps and added mFD as a covariance in the statistical model in the main text (Yan et al. 2013). This method has been found to perform well in removing motion artifacts (Yan et al. 2013). Besides, we also conducted the scrubbing method in a separate analysis to validate our major findings through censoring volumes within each subject's fMRI time series that were associated with sudden head motion (Power et al. 2012). For each subject, an fMRI volume was censored when its FD was above 1 mm. One volume before and 2 volumes after the bad volume were also discarded. One subject was further excluded because less than half of the volumes were remained according to the above criteria. A total of 39 subjects all have more than 112 volumes (~ 3 min, 112–195 volumes, mean \pm SD: 179.2 ± 20.0) of BOLD data remained after motion censoring. We recalculated the age effects on the FCS and network topological properties using censored time courses.

Validation Analysis

To evaluate the reproducibility of our results, we examined the influences of different image preprocessing and network analysis strategies (e.g., global signal removal, different connectivity density thresholds, and weighted network analysis). Briefly, 1) given that global signal of the whole brain is an important confounding factor for brain network analyses based on R-fMRI (Fox et al. 2009; Murphy et al. 2009; Weissenbacher et al. 2009), we thus explored the influences of global signal regression on the major findings; 2) given that the connectivity density may impact the network topological structure, we also examined the findings under other network densities (3 and 7%); 3) given that the weights of connections may provide additional information, we validated the influence of weighted network analysis on our findings. Specifically, the weights of connections survived after thresholding with a density of 5% were applied, and the weighted networks were divided by the mean of the total connection weights. The resultant networks were used for further computation.

Results

Development of Functional Connectivity

With the measurements of FCS from 31.3 to 41.7 weeks, we found that both the mean and the heterogeneity of the FCS across the entire brain increased significantly with age ($t = 3.70$, $P < 0.001$, adjusted $R^2 = 0.28$; $t = 3.20$, $P = 0.003$, adjusted $R^2 = 0.22$, respectively; Fig. 1A). Brain regions with the most significant age-dependent increases in FCS were mainly distributed in the primary sensorimotor, visual, auditory, and language (Wernicke's area, Broca's area, and Rolandic operculum) cortex, as well as subcortical regions (caudate, thalamus, and putamen) (corrected $P < 0.05$; Fig. 1B). We also found increased FCS in a few brain regions involved in default-mode (e.g., ventral medial prefrontal, posterior cingulate, and precuneus) and executive-control (e.g., dorsal anterior cingulate cortex, left lateral prefrontal cortex, and left

inferior parietal lobe) networks (corrected $P < 0.05$; Fig. 1B). The spatial patterns of FCS distribution during development from 31 to 41 weeks are illustrated in Figure 1C and [Supplementary Movie 1](#). The mean FCS pattern of infants scanned at term-equivalent age was also shown as a reference (Fig. 1C). To further understand the spatial range of the connectivity that significantly increases during the developmental period from 31.3 to 41.7 weeks, we computed age-related FCS alterations across different distance bins. The age-related FCS increases were found primarily contributed by the short-to-middle distance connections (10–70 mm, $P < 0.05$, corrected, Fig. 1D). The brain regions with significant FCS increase in short-to-middle connections (Fig. 1D) were spatially similar to those of all-range FCS increases (Fig. 1B). Significant long-distance (70–110 mm) FCS increases were observed in only a few brain regions (Fig. 1D).

Figure 2 shows whole-brain functional connectivity maps with the regions characterized by significantly age-dependent changes as seeds. During development, the thalamus showed increased positive connectivity with sensorimotor and visual regions and increased negative connectivity with PCC/PCu (Fig. 2A). Notably, the significant negative correlation between thalamus and PCC/PCu did not appear until about 38 weeks. The left lingual gyrus showed significantly increased positive connectivity with other regions in visual system and with auditory, language, and sensorimotor regions as well as medial prefrontal cortex (mPFC) (Fig. 2B). Precentral gyrus, a region in the primary sensorimotor system, showed significantly increased positive correlation with contralateral sensorimotor regions and with regions in visual auditory and language systems (Fig. 2C). We found that the regions with significant correlations with PCC/PCu became more focal and the strength of connectivity of these regions to sensorimotor regions decreased with age (Fig. 2D). Additionally, we noticed that the PCC/PCu showed a trend toward age-related increase in functional connections with mPFC (where this increase reached the height threshold but did not survive extent threshold after multiple comparison

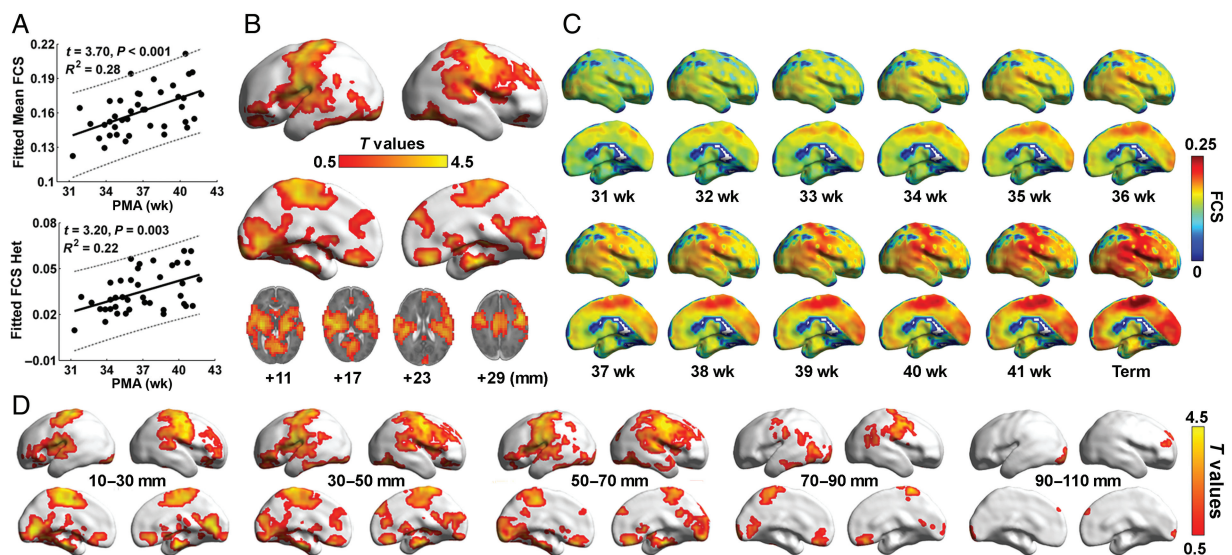


Figure 1. Age-dependent changes in FCS from 31.3 to 41.7 weeks. (A) The mean FCS and the heterogeneity of FCS increased with age. The line plots show the regression line with 95% prediction error bounds. (B) Age effects on nodal FCS. (C) Developing nodal FCS from 31 to 41 weeks demonstrating age-dependent gradual increase of nodal FCS. A map of FCS averaged from 10 term infants (>38.7 weeks at birth) was also presented as a reference. Nodal FCS was calculated as the fitted values of the general linear model with gender and head motion parameters mFD as covariates. (D) Age effects on nodal FCS differentiated within different distance bins. The values were mapped onto the cortical surface using BrainNet Viewer (Xia et al. 2013). The R^2 values were adjusted using gender and mFD as covariates. PMA (weeks), postmenstrual age in weeks; FCS, functional connectivity strength; Het, heterogeneity.

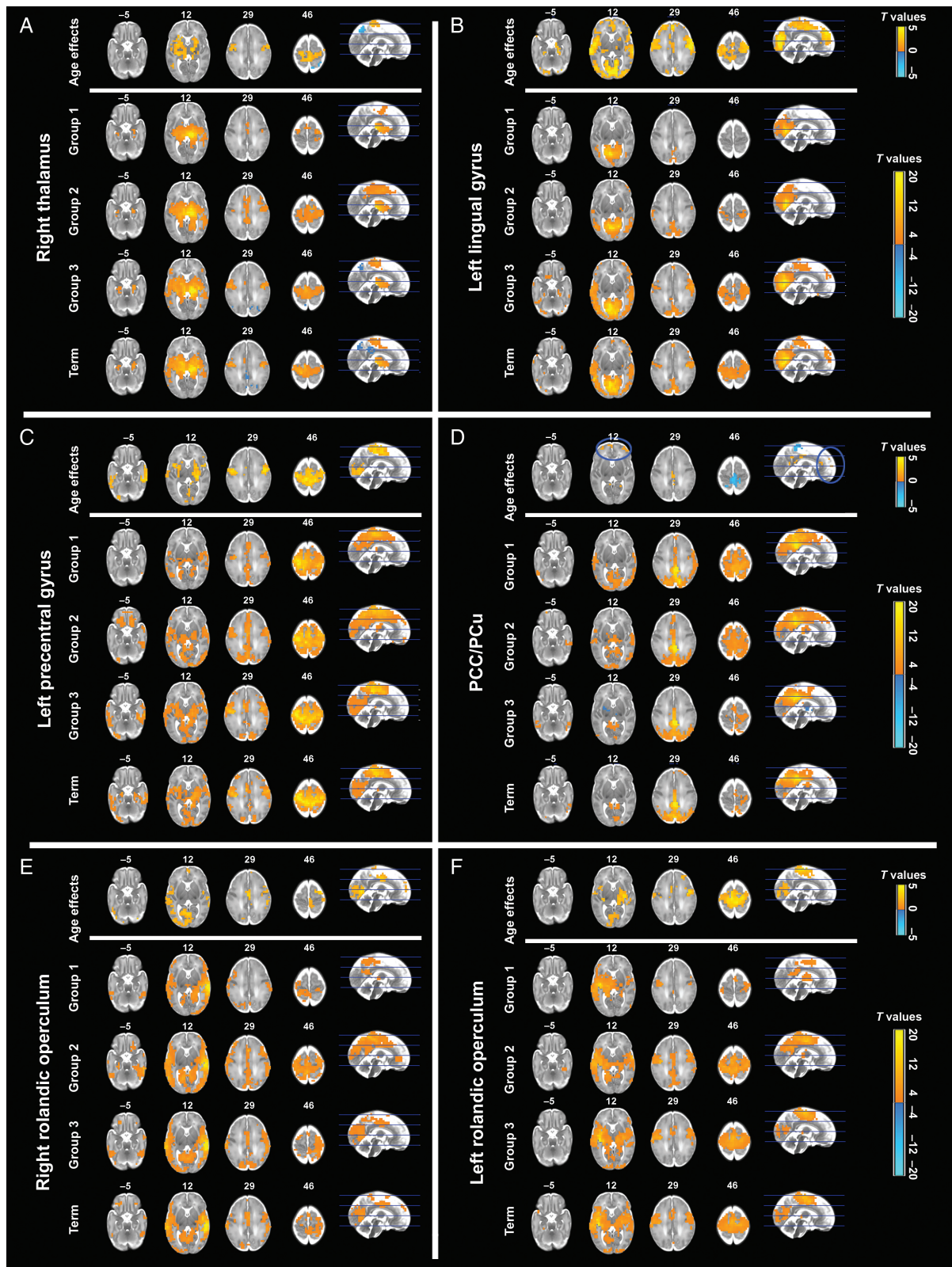


Figure 2. Developmental changes of seed-based functional connectivity. (A) Right thalamus; (B) left lingual gyrus; (C) left precentral gyrus; (D) PCC/PCu; (E) Right rolandic operculum; (F) left rolandic operculum. For each seed ROI, the first row showed the regions with significant age effects on seed-based functional connectivity in axial slices. The 4 rows below showed the regions with significant functional connectivity with the seed regions within 3 different age groups of infants and within a group of term controls (>38.7 weeks at birth, $n = 10$) at a relatively strict threshold of a corrected $P < 0.01$ (which corresponded to an uncorrected single voxel significance level of $P < 0.01$ and a minimum cluster size of 351 mm^3). Representative axial slices for spatial patterns of connectivity are overlaid onto the customized template. PCC/PCu, posterior cingulate/precuneus cortex; MPFC, medial prefrontal cortex; ROI, region of interest.

correction) (Fig. 2D). Bilateral rolandic operculum showed age-related positive correlations with language, sensorimotor, and visual regions (Fig. 2E,F). However, the left rolandic operculum showed stronger positive correlations with the contralateral and sensorimotor regions, possibly indicating that the lateralization was taking place during the third trimester (Fig. 2F).

Development of Network Topology: Global Properties, Hubs and Rich-Club Structure

Small-World and Modular Structure

We found that the C_p , L_p , and $Lamda$ all increased significantly with postmenstrual age ($t = 2.89$, $P = 0.006$, adjusted $R^2 = 0.19$ for C_p ; $t = 2.99$, $P = 0.005$, adjusted $R^2 = 0.20$ for L_p ; $t = 2.90$, $P = 0.006$, adjusted $R^2 = 0.19$ for $Lamda$, respectively; Fig. 3A–C). These results suggest enhanced segregation in brain network organization during this early developmental period. No significant age-related changes in the Γ or Σ were detected ($P_s > 0.05$). Notably, the functional brain networks of all preterm and term babies showed small-world organization, indicating the appearance of small-world properties as early as 31.3 weeks and the persistence of an efficient organization for information transformation from 31.3 to 41.7 weeks (Σ : 1.17–1.67, mean/SD: 1.45/0.12). On the basis of modularity analysis, we observed that the infant brains exhibited significant modular structures but did not display age-related changes in either modularity values or community number (Q : 0.23–0.43, mean/SD: 0.34/0.05; number of modules: 3–7, mean/SD: 5.15/0.86, both $P_s > 0.05$). Notably, both the mean participation coefficients and the number of connectors decreased with age. These findings suggested that while the modular structure was maintained, the increased specificity of modular systems was taking place ($t = -2.60$, $P = 0.014$, adjusted $R^2 = 0.16$; $t = -2.07$, $P = 0.046$, adjusted $R^2 = 0.11$, respectively; Fig. 3D,E).

Nodal Centrality

During this developmental stage, significant age-related increases in the nodal degree values were primarily distributed in

the precentral and postcentral gyri and supplementary motor area, while the decreases were in the posterior cingulate and precuneus cortex (Fig. 4A). Figure 4B illustrates the fitted degree distribution maps of infant brains from 31 to 41 weeks and the mean degree maps of infants scanned at term-equivalent age. The heterogeneity of the nodal degree values increased with age, indicating that the topological roles of nodes in information communication become more diverse with age ($t = 2.73$, $P = 0.01$, adjusted $R^2 = 0.17$; Fig. 4C). We further observed the number of brain hubs increased with age ($t = 3.19$, $P = 0.003$, adjusted $R^2 = 0.22$; Fig. 4D), consistent with which is that only a few regions located in the supplementary motor area and visual cortex were hubs at the very early preterm age (e.g., 31 weeks), while more regions, including the precentral and postcentral gyri and rolandic operculum, emerged as hubs at about 34 weeks and continuously extended and strengthened with development (Fig. 4B). The degree distributions $P(k)$ of the brain networks were best fitted as exponentially truncated power law (Fig. 4E). With the lower exponential degree cut-off values increased significantly with age ($t = 2.36$, $P = 0.024$, adjusted $R^2 = 0.14$; Fig. 4F), the transition from the scaling regimen to the exponential fall-off occurred at a higher degree in older babies, reflecting relative increases in the numbers and connections of hubs in the brain networks with early development.

With the measurement of 3 additional nodal centrality parameters, we found that significant age-related increases in the nodal clustering coefficient were primarily distributed in the supplementary motor area, precentral gyrus, postcentral gyrus, insula, thalamus, and visual cortex ($P < 0.05$, corrected, Fig. 5A). In most of these regions, the participation coefficient values decreased during development ($P < 0.05$, corrected, Fig. 5B). The regions showing age-related decreases in nodal efficiency included the insula, posterior cingulate, precuneus, lateral prefrontal and parietal, dorsal anterior cingulate, and lateral temporal cortices ($P < 0.05$, corrected, Fig. 5C). These findings provide further evidences for enhanced segregation processing and decreased network integrity during development.

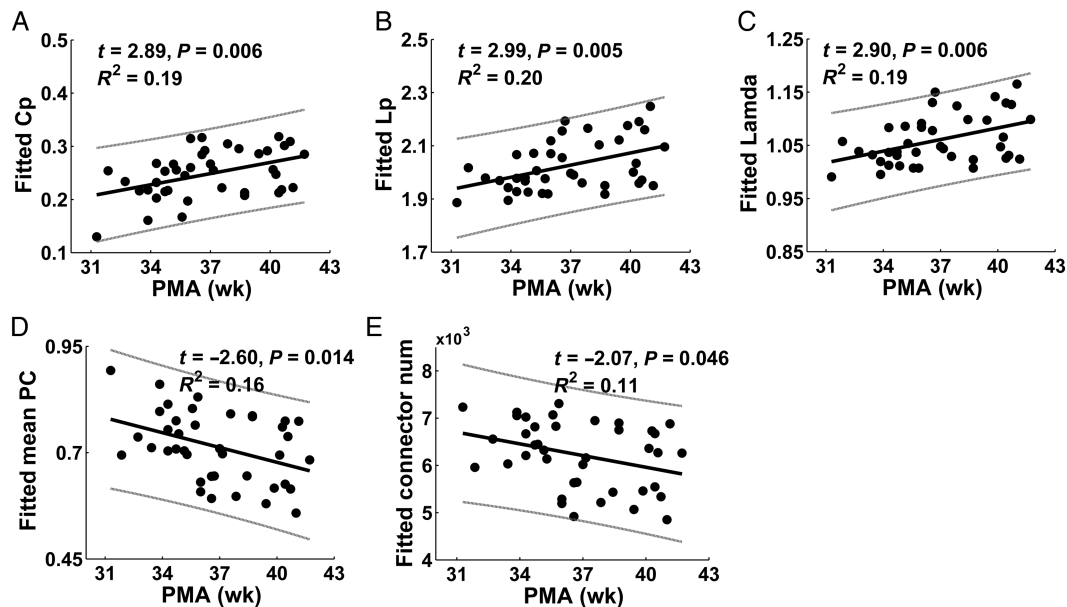


Figure 3. Age-dependent changes of small-world and modular properties from 31.3 to 41.7 weeks. The (A) C_p , (B) L_p , (C) $Lamda$ increased with age. The (D) mean PC and (E) number of connectors (nodes with $PC > 0.45$) decreased with age. The scatter plots show the regression line with 95% prediction error bounds. The R^2 values were adjusted using gender and mFD as covariates. PMA (weeks), postmenstrual age in weeks; Num, number.

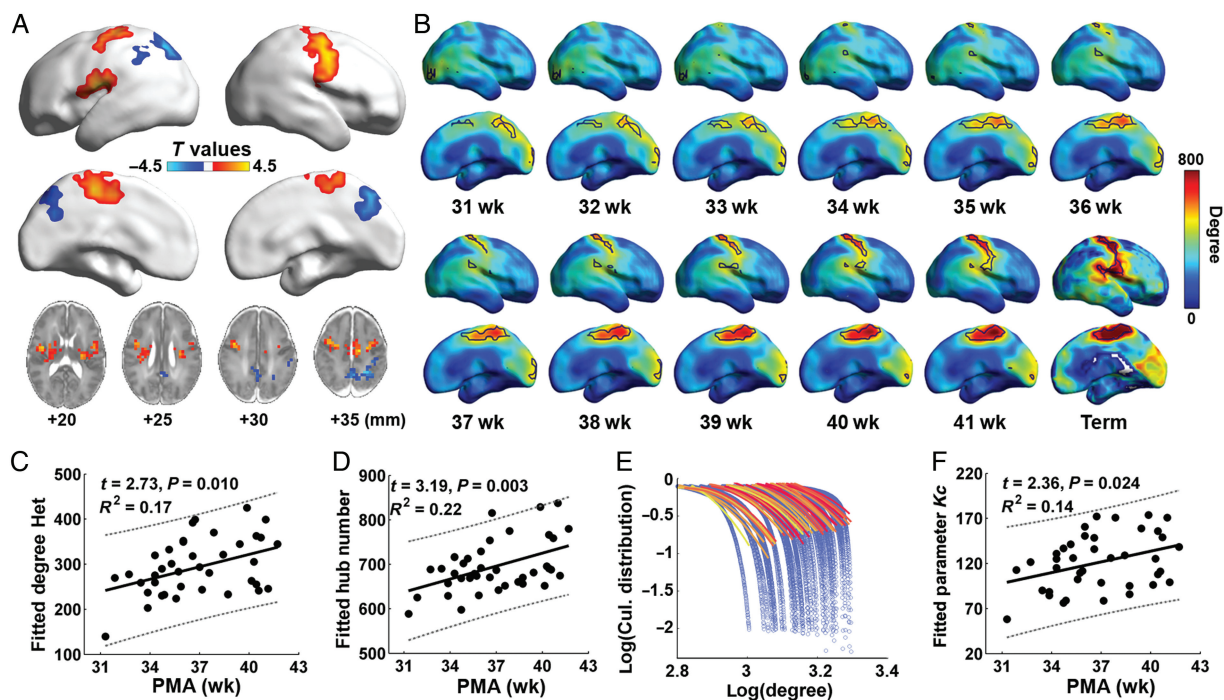


Figure 4. Developmental changes in nodal degree and degree distribution from 31.3 to 41.7 weeks. (A) Regions showing significant age-related changes in nodal degree. (B) The fitted degree map of each week of postmenstrual age. The hubs are delineated with blue lines. The map of nodal degree values averaged from 10 term infants (>38.7 weeks at birth) is also presented as a reference. (C) The heterogeneity of nodal degree increased with age. (D) The number of hubs increased with age. The hubs included regions with nodal degrees > 1.5 SD beyond the mean. (E) The cumulative distributions of degree for each subject. The blue circles indicate the original data. The solid lines indicate the best fitted distributions. The yellow to red colors correspond to ages from younger to older. (F) The distribution parameters (k_c) significantly increased with age. For (C), (D), and (F), the R^2 values were adjusted using gender and mFD as covariates; the dashed lines are the regression lines with 95% prediction error bounds. PMA (weeks), postmenstrual age in weeks; Het, heterogeneity; Cul, cumulative. The values were mapped onto the cortical surface using BrainNet Viewer (Xia et al. 2013).

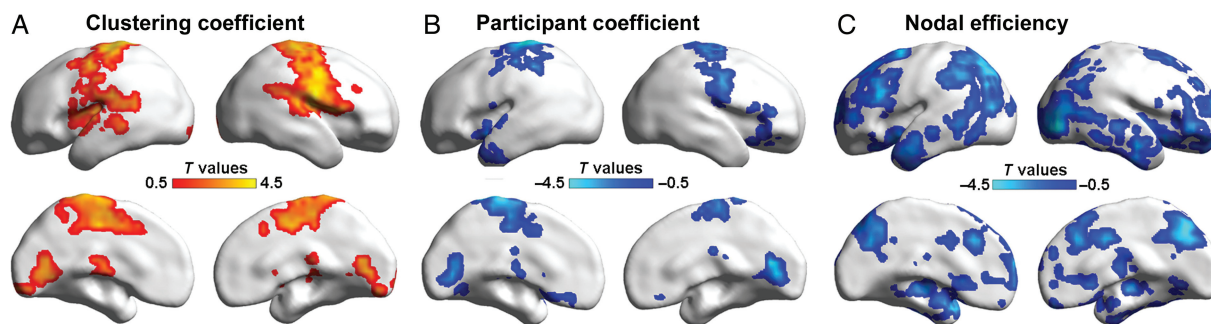


Figure 5. Statistical maps showing regions with significant developmental changes in the (A) nodal clustering coefficient, (B) participation coefficient, and (C) nodal efficiency. The values were mapped onto the cortical surface using BrainNet Viewer (Xia et al. 2013).

Rich-Club Structure

We observed that over the age range examined, the brain connectomes exhibited rich-club structure characterized by normalized Φ values significantly >1 (Fig. 6A). After selecting the illustrated rich club as the one with the highest normalized Φ in each subject, we found that the size of the rich club increased with age ($t = 2.72$, $P = 0.010$, adjusted $R^2 = 0.17$; Fig. 6B). However, the normalized Φ decreased with age, likely reflecting the dramatic expansion of rich-club organization ($t = -3.30$, $P = 0.002$, adjusted $R^2 = 0.24$; Fig. 6C). The spatial changing patterns of rich-club organization were similar to those of the hubs (Fig. 6D,B). According to the categories of the associated nodes, all brain connections could be classified into rich club, feeder, or local edges (van den Heuvel and Sporns 2011; van den Heuvel et al. 2012) (Fig. 6E). We observed that the rich club and feeder connections exhibited

age-related increases or increasing tendency in both number and strength with age (for number: $t = 2.99$, $P = 0.005$, adjusted $R^2 = 0.20$; $t = 2.15$, $P = 0.039$, adjusted $R^2 = 0.12$, respectively; Fig. 6F; for strength: $t = 1.65$, $P = 0.109$, adjusted $R^2 = 0.07$; $t = 3.25$, $P = 0.002$, adjusted $R^2 = 0.23$, respectively; Fig. 6G). For the local connections, we found that the numbers decreased with age, whereas the connectivity strength increased with age ($t = -2.79$, $P = 0.008$, adjusted $R^2 = 0.18$, Fig. 6F; $t = 3.57$, $P = 0.001$, adjusted $R^2 = 0.27$, respectively, Fig. 6G).

Prediction of Brain Maturity Using Functional Connectomic Measurements

Using the support vector regression and leave-one-out cross-validation, we found that the nodal FCS was able to significantly

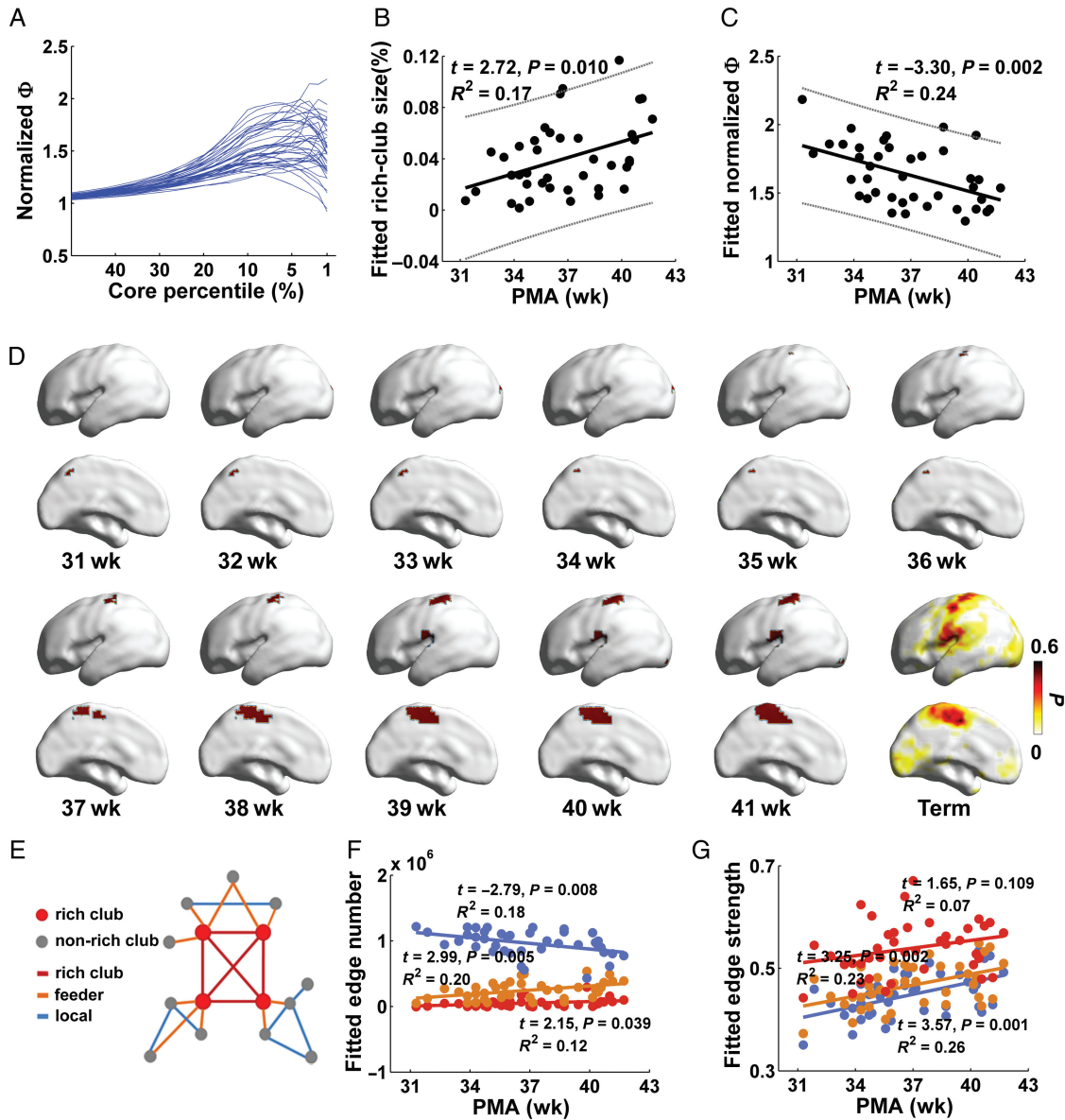


Figure 6. Development of rich-club organization from 31.3 to 41.7 weeks. (A) Individual normalized rich-club curves (Φ_{norm}) for each baby. (B) The size of rich club and (C) the normalized rich-club coefficients significantly changed with age. (D) Maps showing the membership probabilities of regions belonging to the rich-club organization at each week of postmenstrual age. Rich-club probability map of 10 term infants (>38.7 weeks at birth) is also presented. (E) An illustration figure of the rich-club organization. The age-related changes in (F) edge number and (G) edge strength of different types of connections (rich club, feeder, and local connections) are shown. The R^2 values were adjusted using gender and mFD as covariates; the dashed lines are the regression lines with 95% prediction error bounds. PMA (weeks), postmenstrual age in weeks. The values were mapped onto the cortical surface using BrainNet Viewer (Xia et al. 2013).

($r = 0.58$, $P < 0.001$; Fig. 7A) predict the brain age, and that the regions with high prediction power were mainly located at the posterior cingulate, precuneus, medial prefrontal, visual cortex, medial temporal, and sensorimotor regions (Fig. 7B). For whole-brain network metrics, although there were not any single measurement showing prediction power ($P_s > 0.05$), the combined one was able to predict the brain age ($r = 0.15$, $P = 0.007$).

Validation Results

We evaluated the effects of head motion and different processing strategies on our main findings. For functional connectivity strength analyses, we found that the previous conclusions remained unchanged under both head motion scrubbing and

global signal removal (Fig. 8A,B). Notably, although the visual cortex and executive-control regions exhibited nonsignificant results with global signal removal, these regions reached the height threshold but did not survive thresholding after multiple comparison correction. For the topological metrics of functional connectome, we found our main results were remained under head motion correction and different processing strategies. 1) Head motion scrubbing. We also observed significantly increased C_p , L_p , and L_{mda} with development using the scrubbed data ($t = 3.57$, $P = 0.001$, adjusted $R^2 = 0.27$; $t = 3.49$, $P = 0.001$, adjusted $R^2 = 0.26$; $t = 3.46$, $P = 0.001$, adjusted $R^2 = 0.26$; respectively; Fig. 9A). 2) Connectivity density (3 and 7%) analysis. Most of the major findings (connectivity density = 5%) remained unchanged including the increased C_p , L_p , and L_{mda} with development

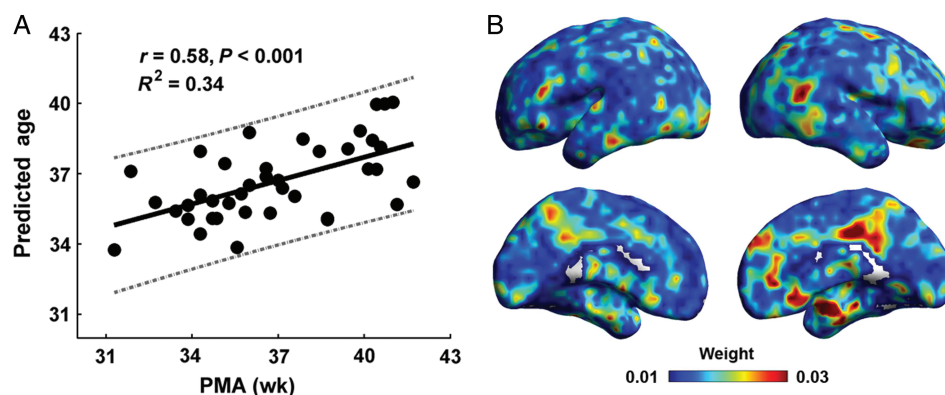


Figure 7. The prediction results of individual brain age based on nodal FCS. (A) The prediction results of nodal FCS. The scatter plots show the correlation line of actual versus predicted age with 95% confidence interval. Pearson correlation coefficient between the actual and predicted ages was calculated to assess the prediction accuracy. Ten thousand permutation tests were performed to determine the statistical significance. (B) Absolute weighting map of support vector regression analysis to predict brain age using FCS. The values were mapped onto the cortical surface using BrainNet Viewer (Xia et al. 2013).

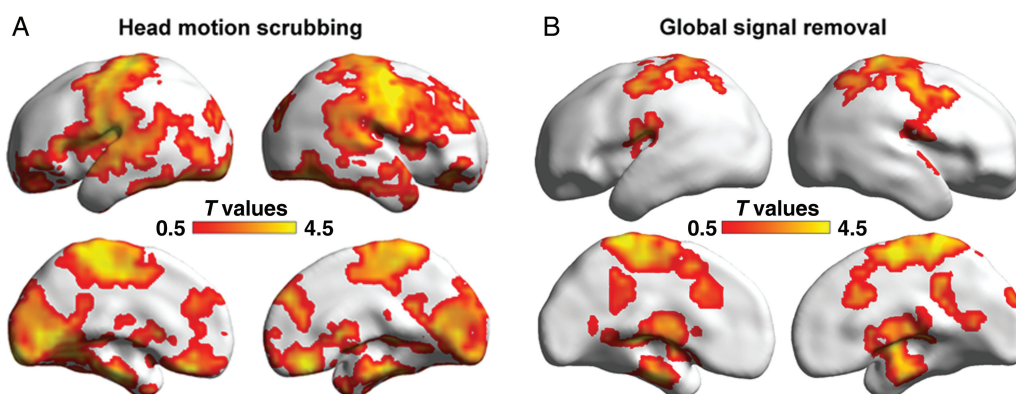


Figure 8. Developmental changes of nodal functional connectivity strength (FCS) with data after global signal removal and with data after head motion scrubbing. The FCS values were mapped onto the cortical surface using BrainNet Viewer (Xia et al. 2013).

under 2 other densities (3 and 7%; Fig. 9B). Additionally, we also found age-related decreases of Σ under a density of 3% ($t = -2.09$, $P = 0.044$, adjusted $R^2 = 0.11$). 3) Weighted network analysis. We also observed similar findings including the increased C_p , L_p , and Λ with development ($t = 3.54$, $P = 0.001$, adjusted $R^2 = 0.26$; $t = 2.93$, $P = 0.006$, adjusted $R^2 = 0.20$; $t = 2.37$, $P = 0.024$, adjusted $R^2 = 0.14$; respectively) while other properties showed no significant age effects (Fig. 9C).

Discussion

By systematically investigating the early development of human brain functional connectome during the third trimester from 31.3 to 41.7 weeks, we found disproportional increases of functional connectivity strength mainly distributed in the primary sensorimotor, visual, and language regions and reflected largely by enhancement of short-to-middle range connections. For the connectomic architecture, while small-world, modular, and rich-club structures were present at 31.3 weeks, local clustering and the shortest path length increased gradually and rich-club structure expanded from 31.3 to 41.7 weeks, resulting in the architectural transformation from a relatively random to more organized configuration. We also found that the functional connectomic metrics could predict the individual brain maturity. Together, these findings suggested gradual enhancement of functional segregation in the brain networks in the third trimester, which

is primarily driven by the rapid growth of functional connectivity and hubs of the primary regions.

Strength and Heterogeneity of Functional Connectivity Increased with Age

Using seed-based (Smyser et al. 2010; Thomason et al. 2013, 2015; Jakab et al. 2014) and independent component analysis (Doria et al. 2010; Toulmin et al. 2015) methods, several previous R-fMRI studies on both fetuses and preterm infants have reported the development of connectivity in regions involving primary visual, sensorimotor, auditory, and subcortical networks and higher order networks, such as default-mode network (DMN). Whole brain voxel-wise analysis in this study is computationally expensive, but could readily reveal the elaborate connectivity changes during the early developmental period, which were not well characterized previously. We found that these short-to-middle range connections are major contributors to significant functional connectivity increases in primary brain regions during the early developmental period (Fig. 1). The dominant development of primary regions prior to birth, supported by the drastic increase of short-to-middle range connections among them, could be helpful for basic survival functions by the time of birth and might lead to the low variability of functional organization in these regions across adult subjects (Buckner and Krienen 2013; Mueller et al. 2013). In contrast, the development

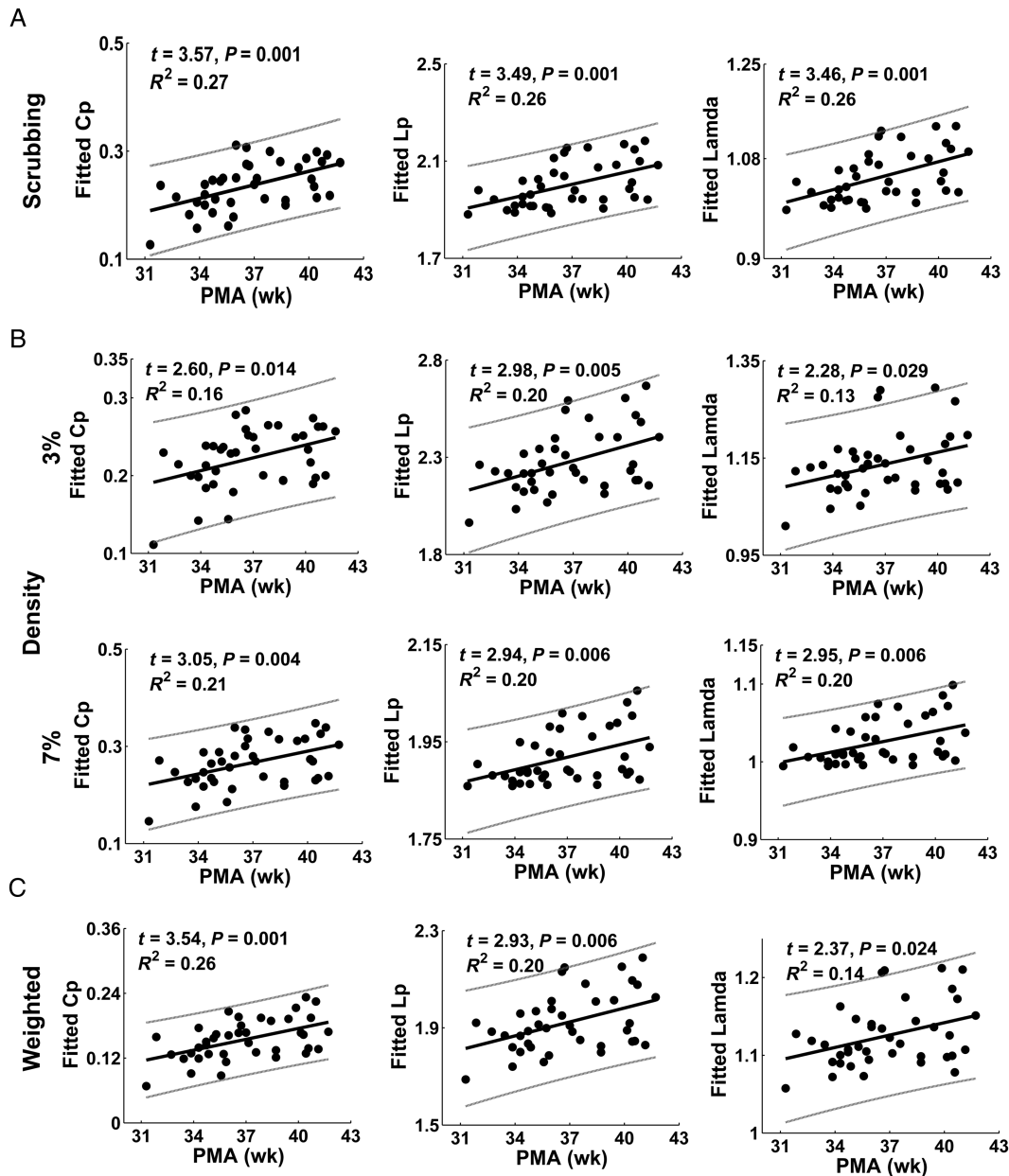


Figure 9. Age-dependent changes of C_p , L_p , and $Lamda$ from 31.3 to 41.3 weeks with head motion scrubbing and different processing strategies. (A) Data after head motion scrubbing. (B) Different densities (3 and 7%). (C) Weighted brain networks. The scatter plots show the regression line with 95% prediction error bounds. The R^2 values were adjusted with gender and mFD as covariates. PMA (weeks), postmenstrual age in weeks.

of long-range connections, primarily involved in global information integration, mostly occurs after birth (Fair et al. 2009; Supekar et al. 2009; Dosenbach et al. 2010; Gao et al. 2011). The disproportionate increase of FCS in primary systems is also associated with the significantly increased heterogeneity of regional connectivity strength and increased degree heterogeneity (Figs 1A and 4C), indicating increased complexity in both local brain regions and global brain networks with development. These findings are compatible with a previous report that prematurity in infants leads to a reduction in the complexity of R-fMRI covariance structure (Smyser et al. 2016).

Seed-based connectivity analysis revealed detailed maps of the regions (Fig. 2) where BOLD signals were positively or negatively correlated to the regions with most significant age-

dependent FCS changes. We observed that both within- and between-system connectivity changed significantly with age for sensorimotor, visual, and language systems. The DMN was found to be more concentrated in PCC/PCu, whereas increased anterior-posterior connections within DMN were also detected, suggesting that the development of higher order functional network was taking place during the third trimester. Besides corticocortical connectivity, we also found significant changes in thalamocortical connectivity, which were reflected by increased connections between thalamus and sensorimotor cortex and decreased connections between thalamus and heteromodal cortex, consistent with previous findings about the early development of thalamocortical connectivity (Toulmin et al. 2015; Ball et al. 2016). Although both corticocortical and thalamocortical age-dependent

connectivity changes were detected, the results in this study demonstrated that the widespread corticocortical connectivity changes were dominant at this phase, and these changes could be attributable to the drastically macrostructural (Dubois et al. 2008) and microstructural (Yu et al. 2015) development of cortical plate during the third trimester.

Developed Functional Specialization with Increased Segregation Process in Brain Networks

Another key finding in the present study was the increased functional specificity in the preterm human brain from 31.3 to 41.7 weeks from a graph theory perspective. The small-worldness was observed to exist across the studied age period, reflecting the emergence of functional segregation and integration pattern. Nonetheless, we found significantly increased clustering coefficient and characteristic shortest path length in the brain networks with age, suggesting a gradually enhanced functional segregation of information processing (Fig. 3). Furthermore, we observed decreases in the participation coefficients and number of connectors with the modular analysis (Fig. 3). These results indicated that the connections became more locally clustered, underlying early differentiation of the functional networks. Another R-fMRI study (Wylie et al. 2014) using independent component analysis suggested that functional segregation continues after birth into childhood. The specialization process has also been found with EEG (Vanhatalo and Kaila 2006). Notably, the development of brain specialization showed a good correspondence with behavioral development. For example, Werner's "orthogenetic principle" suggested that increased differentiation and hierarchical organization of behavior occur during child development (Werner 1957; Sameroff 2010). The interactive specialization framework (Johnson 2000) predicted that both networks and regions within networks become more functionally specialized or segregated as they mature.

Strengthened Hub and Rich-Club Structures

We demonstrated strengthened functional hubs in brain networks during early development. Even in the brain of very early preterm babies, the hubs were found to appear at locations primarily in the supplementary motor areas and few visual regions, which are distinct to those of adults in the postero-medial cores with extensions into the temporo-parietal junction and fronto-medial cortices (Buckner et al. 2009; Zuo et al. 2012; Liang et al. 2013; van den Heuvel and Sporns 2013). The presence of hub structure in such an early phase indicates that the brain functional networks were already nonrandom with different regions playing heterogeneous roles in information communication. During early development, the number of brain hubs increased significantly and hub regions were additionally found in primary sensory, motor, and visual regions and Wernicke's area (Fig. 4B), converging with the previous findings in neonates born full term (Fransson et al. 2011). The primary sensory regions exhibited the highest degree of glucose metabolism in infant brains at term (Chugani et al. 1987; Chugani 1998). Previous studies on adults suggested that higher rates of cerebral blood flow and metabolism activity occurred at the hubs (Liang et al. 2013; Tomasi et al. 2014). Notably, similar to both the functional and structural networks of adults (Achard et al. 2006; He et al. 2007; Gong et al. 2009), the degree distribution of all infants followed exponentially truncated power law (Fig. 4E), suggesting that specific physical rules were topologically obeyed even in preterm brains. Specifically, these rules facilitated the existence of hubs and prevent the

appearance of nodes with extremely high centrality to maintain high communication abilities and high attack resilience. Remarkably, the rich-club organization, a phenomenon of densely interconnected hubs, already appeared at 31.3 weeks and expanded in size with age (Fig. 6). The locations of hubs and rich clubs identified in the functional networks in this study were slightly different from those in the structural connectomes in preterm and term infants (Shi et al. 2012; Ball et al. 2014; Brown et al. 2014; van den Heuvel et al. 2015; Huang et al. 2015). These discrepancies probably indicate differences in maturation between functional and structural connectomes (van den Heuvel and Sporns 2013). Finally, it is noteworthy that the preterm effects on the subsequent hub and rich-club distribution changes during development cannot be addressed in this study without longitudinal R-fMRI data of both preterm-born and term-born infants (more preterm effects in the discussion below).

Limitations, Technical Considerations, and Future Directions

Several further issues need to be considered. First, preterm birth has been associated with adverse neurodevelopmental outcomes (Woodward et al. 2006). Despite that, MRI examinations of preterm infants have been predominantly used to understand brain development during the third trimester. Accumulated studies using R-fMRI indicated dramatic reconfiguration during the last 10 weeks prior to normal time of birth (Fransson et al. 2007, 2009; Doria et al. 2010; Smyser et al. 2010). Exposure to the extrauterine environment could be one of the factors underlying the observed network reorganization, but these effects would be relatively subtle compared with the dramatic developmental factor during the third trimester (Bourgeois et al. 1989; Kostovic 1990). Nevertheless, it is likely that the disruption of the network could become apparent in years subsequent to premature birth. Second, there are growing interests on the influence of gut microbiota on brain development. The microbiome of the infants is likely to be affected by many factors such as the mode of delivery (vaginal vs. C-section), feeding practices (breast-feeding vs. formula), and exposure to antibiotic during pregnancy via maternal microbiota (Borre et al. 2014). Specifically, preterm-born infants are at greater risk for marked dysbiosis of the gut microbiota. In the future, it would be very interesting to explore how gut microbiota affects brain development in babies. Third, given that the global signal removal is associated with the emergence of negative correlations, which are still difficult to interpret (Fox et al. 2009; Murphy et al. 2009; Weissenbacher et al. 2009), we did not regress out the global signal in the data analysis for the main results. For validation, global signal removal was also conducted and similar age-related increases in the FCS were detected in all regions but the visual cortex (Fig. 8B). These results were consistent with previous findings that global signal regression reduces the significant correlations in visual regions (Murphy et al. 2009; Chai et al. 2012). Fourth, considering recent concerns about the motion-induced spurious findings on functional connectivity, we processed the R-fMRI data with Friston's 24-parameter regression and used the *mFD* parameter as a covariant in the GLM to regress out head motion effects. Validation with scrubbing analysis showed that the major results were largely preserved (Figs 8A,9A) (Power et al. 2012). Fifth, previous studies have reported the complex relationship between the structural and functional networks in adult brains (Wang et al. 2015). However, this relationship during the very early developmental stage remains elusive and needs further exploration. Finally, future longitudinal studies, instead of cross-sectional studies, would

better delineate these early developmental trajectories of human brain connectomes in preterm development.

Supplementary Material

Supplementary material can be found at: <http://www.cercor.oxfordjournals.org/>.

Funding

This study is financially sponsored through NIH (Grant Nos. R01MH092535, U54HD086984 and R01MH092535-S1 to H.H.), the National Science Fund for Distinguished Young Scholars (Grant No 81225012), the Natural Science Foundation of China (Grant Nos. 91432115 and 31221003), the 111 Project (Grant No. B07008), and the Open Research Fund of the State Key Laboratory of Cognitive Neuroscience and Learning (Grant No. CNLYB1407 to Y.H. and H.H.).

Notes

Conflict of Interest: None declared.

References

- Achard S, Bullmore E. 2007. Efficiency and cost of economical brain functional networks. *PLoS Comput Biol.* 3:e17.
- Achard S, Salvador R, Whitcher B, Suckling J, Bullmore E. 2006. A resilient, low-frequency, small-world human brain functional network with highly connected association cortical hubs. *J Neurosci.* 26:63–72.
- Ball G, Aljabar P, Arichi T, Tusor N, Cox D, Merchant N, Nongena P, Hajnal JV, Edwards AD, Counsell SJ. 2016. Machine-learning to characterise neonatal functional connectivity in the preterm brain. *Neuroimage.* 124:267–275.
- Ball G, Aljabar P, Zebari S, Tusor N, Arichi T, Merchant N, Robinson EC, Ogunidipe E, Rueckert D, Edwards AD, et al. 2014. Rich-club organization of the newborn human brain. *Proc Natl Acad Sci USA.* 111:7456–7461.
- Biswal B, Yetkin FZ, Haughton VM, Hyde JS. 1995. Functional connectivity in the motor cortex of resting human brain using echo-planar MRI. *Magn Reson Med.* 34:537–541.
- Biswal BB, Mennes M, Zuo XN, Gohel S, Kelly C, Smith SM, Beckmann CF, Adelstein JS, Buckner RL, Colcombe S, et al. 2010. Toward discovery science of human brain function. *Proc Natl Acad Sci USA.* 107:4734–4739.
- Blondel VD, Guillaume J-L, Lambiotte R, Lefebvre E. 2008. Fast unfolding of communities in large networks. *J Stat Mech.* 2008:P10008.
- Borre YE, O’Keeffe GW, Clarke G, Stanton C, Dinan TG, Cryan JF. 2014. Microbiota and neurodevelopmental windows: implications for brain disorders. *Trends Mol Med.* 20:509–518.
- Bourgeois JP, Jastreboff PJ, Rakic P. 1989. Synaptogenesis in visual cortex of normal and preterm monkeys: evidence for intrinsic regulation of synaptic overproduction. *Proc Natl Acad Sci USA.* 86:4297–4301.
- Brown CJ, Miller SP, Booth BG, Andrews S, Chau V, Poskitt KJ, Hamarneh G. 2014. Structural network analysis of brain development in young preterm neonates. *Neuroimage.* 101:667–680.
- Buckner RL, Krienen FM. 2013. The evolution of distributed association networks in the human brain. *Trends Cogn Sci.* 17:648–665.
- Buckner RL, Sepulcre J, Talukdar T, Krienen FM, Liu H, Hedden T, Andrews-Hanna JR, Sperling RA, Johnson KA. 2009. Cortical hubs revealed by intrinsic functional connectivity: mapping, assessment of stability, and relation to Alzheimer’s disease. *J Neurosci.* 29:1860–1873.
- Bullmore E, Sporns O. 2009. Complex brain networks: graph theoretical analysis of structural and functional systems. *Nat Rev Neurosci.* 10:186–198.
- Bullmore E, Sporns O. 2012. The economy of brain network organization. *Nat Rev Neurosci.* 13:336–349.
- Bystron I, Blakemore C, Rakic P. 2008. Development of the human cerebral cortex: Boulder Committee revisited. *Nat Rev Neurosci.* 9:110–122.
- Cao M, Wang JH, Dai ZJ, Cao XY, Jiang LL, Fan FM, Song XW, Xia MR, Shu N, Dong Q, et al. 2014. Topological organization of the human brain functional connectome across the life-span. *Dev Cogn Neurosci.* 7:76–93.
- Chai XJ, Castañón AN, Öngür D, Whitfield-Gabrieli S. 2012. Anticorrelations in resting state networks without global signal regression. *Neuroimage.* 59:1420–1428.
- Chugani HT. 1998. A critical period of brain development: studies of cerebral glucose utilization with PET. *Prev Med.* 27:184–188.
- Chugani HT, Phelps ME, Mazziotta JC. 1987. Positron emission tomography study of human brain functional development. *Ann Neurol.* 22:487–497.
- Dehaene-Lambertz G, Spelke ES. 2015. The infancy of the human brain. *Neuron.* 88:93–109.
- Di Martino A, Fair DA, Kelly C, Satterthwaite TD, Castellanos FX, Thomason ME, Craddock RC, Luna B, Leventhal BL, Zuo XN, et al. 2014. Unraveling the miswired connectome: a developmental perspective. *Neuron.* 83:1335–1353.
- Doria V, Beckmann CF, Arichi T, Merchant N, Groppo M, Turkheimer FE, Counsell SJ, Murgasova M, Aljabar P, Nunes RG, et al. 2010. Emergence of resting state networks in the preterm human brain. *Proc Natl Acad Sci USA.* 107:20015–20020.
- Dosenbach NU, Nardos B, Cohen AL, Fair DA, Power JD, Church JA, Nelson SM, Wig GS, Vogel AC, Lessov-Schlaggar CN, et al. 2010. Prediction of individual brain maturity using fMRI. *Science.* 329:1358–1361.
- Dubois J, Dehaene-Lambertz G, Perrin M, Mangin JF, Cointepas Y, Duchesnay E, Le Bihan D, Hertz-Pannier L. 2008. Asynchrony of the early maturation of white matter bundles in healthy infants: Quantitative landmarks revealed noninvasively by diffusion tensor imaging. *Hum Brain Mapp.* 29:14–27.
- Engle WA. 2004. Age terminology during the perinatal period. *Pediatrics.* 114:1362–1364.
- Fair DA, Cohen AL, Power JD, Dosenbach NU, Church JA, Miezin FM, Schlaggar BL, Petersen SE. 2009. Functional brain networks develop from a “local to distributed” organization. *PLoS Comput Biol.* 5:e1000381.
- Fox MD, Zhang D, Snyder AZ, Raichle ME. 2009. The global signal and observed anticorrelated resting state brain networks. *J Neurophysiol.* 101:3270–3283.
- Fransson P, Aden U, Blennow M, Lagercrantz H. 2011. The functional architecture of the infant brain as revealed by resting-state fMRI. *Cereb Cortex.* 21:145–154.
- Fransson P, Skiold B, Engstrom M, Hallberg B, Mosskin M, Aden U, Lagercrantz H, Blennow M. 2009. Spontaneous brain activity in the newborn brain during natural sleep—an fMRI study in infants born at full term. *Pediatr Res.* 66:301–305.
- Fransson P, Skiold B, Horsch S, Nordell A, Blennow M, Lagercrantz H, Aden U. 2007. Resting-state networks in the infant brain. *Proc Natl Acad Sci USA.* 104:15531–15536.

- Friston KJ. 1994. Functional and effective connectivity in neuroimaging: a synthesis. *Hum Brain Mapp.* 2:56–78.
- Friston KJ, Williams S, Howard R, Frackowiak RS, Turner R. 1996. Movement-related effects in fMRI time-series. *Magn Reson Med.* 35:346–355.
- Gao W, Gilmore JH, Giovanello KS, Smith JK, Shen D, Zhu H, Lin W. 2011. Temporal and spatial evolution of brain network topology during the first two years of life. *PLoS One.* 6:e25278.
- Gong G, He Y, Concha L, Lebel C, Gross DW, Evans AC, Beaulieu C. 2009. Mapping anatomical connectivity patterns of human cerebral cortex using in vivo diffusion tensor imaging tractography. *Cereb Cortex.* 19:524–536.
- He Y, Chen ZJ, Evans AC. 2007. Small-world anatomical networks in the human brain revealed by cortical thickness from MRI. *Cereb Cortex.* 17:2407–2419.
- Huang H, Shu N, Mishra V, Jeon T, Chalak L, Wang ZJ, Rollins N, Gong G, Cheng H, Peng Y, et al. 2015. Development of human brain structural networks through infancy and childhood. *Cereb Cortex.* 25:1389–1404.
- Humphries MD, Gurney K, Prescott TJ. 2005. The brainstem reticular formation is a small world, not scale-free, network. *Proc R Soc Lond B Biol Sci.* 273:503–511.
- Jakab A, Schwartz E, Kasprian G, Gruber GM, Prayer D, Schopf V, Langs G. 2014. Fetal functional imaging portrays heterogeneous development of emerging human brain networks. *Front Hum Neurosci.* 8:852.
- Johnson MH. 2000. Functional brain development in infants: elements of an interactive specialization framework. *Child Dev.* 71:75–81.
- Kelly C, Biswal BB, Craddock RC, Castellanos FX, Milham MP. 2012. Characterizing variation in the functional connectome: promise and pitfalls. *Trends Cogn Sci.* 16:181–188.
- Kostovic I. 1990. Structural and histochemical reorganization of the human prefrontal cortex during perinatal and postnatal life. *Prog Brain Res.* 85:223–239; discussion 239–240.
- Kostovic I, Jovanov-Milosevic N. 2006. The development of cerebral connections during the first 20–45 weeks' gestation. *Semin Fetal Neonatal Med.* 11:415–422.
- Latora V, Marchiori M. 2001. Efficient behavior of small-world networks. *Phys Rev Lett.* 87:198701.
- Ledberg A, Akerman S, Roland PE. 1998. Estimation of the probabilities of 3D clusters in functional brain images. *Neuroimage.* 8:113–128.
- Liang X, Zou Q, He Y, Yang Y. 2013. Coupling of functional connectivity and regional cerebral blood flow reveals a physiological basis for network hubs of the human brain. *Proc Natl Acad Sci USA.* 110:1929–1934.
- Molliver ME, Kostovic I, van der Loos H. 1973. The development of synapses in cerebral cortex of the human fetus. *Brain Res.* 50:403–407.
- Mueller S, Wang D, Fox MD, Yeo BT, Sepulcre J, Sabuncu MR, Shafee R, Lu J, Liu H. 2013. Individual variability in functional connectivity architecture of the human brain. *Neuron.* 77:586–595.
- Murphy K, Birn RM, Handwerker DA, Jones TB, Bandettini PA. 2009. The impact of global signal regression on resting state correlations: are anti-correlated networks introduced? *Neuroimage.* 44:893–905.
- Newman ME. 2006. Modularity and community structure in networks. *Proc Natl Acad Sci USA.* 103:8577–8582.
- Power JD, Barnes KA, Snyder AZ, Schlaggar BL, Petersen SE. 2012. Spurious but systematic correlations in functional connectivity MRI networks arise from subject motion. *Neuroimage.* 59:2142–2154.
- Rakic P. 1972. Mode of cell migration to the superficial layers of fetal monkey neocortex. *J Comp Neurol.* 145:61–83.
- Rakic P. 1995. Radial versus tangential migration of neuronal clones in the developing cerebral cortex. *Proc Natl Acad Sci USA.* 92:11323–11327.
- Salvador R, Suckling J, Coleman MR, Pickard JD, Menon D, Bullmore E. 2005. Neurophysiological architecture of functional magnetic resonance images of human brain. *Cereb Cortex.* 15:1332–1342.
- Sameroff A. 2010. A unified theory of development: a dialectic integration of nature and nurture. *Child Dev.* 81:6–22.
- Serag A, Aljabar P, Ball G, Counsell SJ, Boardman JP, Rutherford MA, Edwards AD, Hajnal JV, Rueckert D. 2012. Construction of a consistent high-definition spatio-temporal atlas of the developing brain using adaptive kernel regression. *Neuroimage.* 59:2255–2265.
- Shi F, Yap PT, Gao W, Lin W, Gilmore JH, Shen D. 2012. Altered structural connectivity in neonates at genetic risk for schizophrenia: a combined study using morphological and white matter networks. *Neuroimage.* 62:1622–1633.
- Sidman RL, Rakic P. 1973. Neuronal migration, with special reference to developing human brain: a review. *Brain Res.* 62:1–35.
- Smyser CD, Inder TE, Shimony JS, Hill JE, Degnan AJ, Snyder AZ, Neil JJ. 2010. Longitudinal analysis of neural network development in preterm infants. *Cereb Cortex.* 20:2852–2862.
- Smyser CD, Snyder AZ, Shimony JS, Mitra A, Inder TE, Neil JJ. 2016. Resting-state network complexity and magnitude are reduced in prematurely born infants. *Cereb Cortex.* 26:322–333.
- Sporns O, Tononi G, Kötter R. 2005. The human connectome: a structural description of the human brain. *PLoS Comput Biol.* 1:e42.
- Supekar K, Musen M, Menon V. 2009. Development of large-scale functional brain networks in children. *PLoS Biol.* 7:e1000157.
- Thomason ME, Dassanayake MT, Shen S, Katkuri Y, Alexis M, Anderson AL, Yeo L, Mody S, Hernandez-Andrade E, Hassan SS, et al. 2013. Cross-hemispheric functional connectivity in the human fetal brain. *Sci Transl Med.* 5:173ra124.
- Thomason ME, Grove LE, Lozon TA Jr, Vila AM, Ye Y, Nye MJ, Manning JH, Pappas A, Hernandez-Andrade E, Yeo L, et al. 2015. Age-related increases in long-range connectivity in fetal functional neural connectivity networks in utero. *Dev Cogn Neurosci.* 11:96–104.
- Tomasi D, Volkow ND. 2011. Functional connectivity hubs in the human brain. *Neuroimage.* 57:908–917.
- Tomasi D, Wang R, Wang GJ, Volkow ND. 2014. Functional connectivity and brain activation: a synergistic approach. *Cereb Cortex.* 24:2619–2629.
- Toulmin H, Beckmann CF, O'Muircheartaigh J, Ball G, Nongena P, Makropoulos A, Ederies A, Counsell SJ, Kennea N, Arichi T, et al. 2015. Specialization and integration of functional thalamocortical connectivity in the human infant. *Proc Natl Acad Sci USA.* 112:6485–6490.
- van den Heuvel MP, Kahn RS, Goni J, Sporns O. 2012. High-cost, high-capacity backbone for global brain communication. *Proc Natl Acad Sci USA.* 109:11372–11377.
- van den Heuvel MP, Kersbergen KJ, de Reus MA, Keunen K, Kahn RS, Groenendaal F, de Vries LS, Benders MJ. 2015. The neonatal connectome during preterm brain development. *Cereb Cortex.* 25:3000–3013.
- van den Heuvel MP, Sporns O. 2013. Network hubs in the human brain. *Trends Cogn Sci.* 17:683–696.

- van den Heuvel MP, Sporns O. 2011. Rich-club organization of the human connectome. *J Neurosci.* 31:15775–15786.
- Vanhatalo S, Kaila K. 2006. Development of neonatal EEG activity: from phenomenology to physiology. *Semin Fetal Neonatal Med.* 11:471–478.
- Wang Y, Du H, Xia M, Ren L, Xu M, Xie T, Gong G, Xu N, Yang H, He Y. 2013. A hybrid CPU-GPU accelerated framework for fast mapping of high-resolution human brain connectome. *PLoS One.* 8:e62789.
- Wang Z, Dai Z, Gong G, Zhou C, He Y. 2015. Understanding structural-functional relationships in the human brain: a large-scale network perspective. *Neuroscientist.* 21:290–305.
- Watts DJ, Strogatz SH. 1998. Collective dynamics of ‘small-world’ networks. *Nature.* 393:440–442.
- Weissenbacher A, Kasess C, Gerstl F, Lanzenberger R, Moser E, Windischberger C. 2009. Correlations and anticorrelations in resting-state functional connectivity MRI: a quantitative comparison of preprocessing strategies. *Neuroimage.* 47:1408–1416.
- Werner H. 1957. The concept of development from a comparative and organismic point of view. In: Harris DB, editor. *The concept of development.* University of Minnesota Press. p. 126.
- Woodward LJ, Anderson PJ, Austin NC, Howard K, Inder TE. 2006. Neonatal MRI to predict neurodevelopmental outcomes in preterm infants. *New Engl J Med.* 355:685–694.
- Wylie KP, Rojas DC, Ross RG, Hunter SK, Maharajh K, Cornier MA, Tregellas JR. 2014. Reduced brain resting-state network specificity in infants compared with adults. *Neuropsychiatr Dis Treat.* 10:1349–1359.
- Xia M, Wang J, He Y. 2013. BrainNet Viewer: a network visualization tool for human brain connectomics. *PLoS One.* 8:e68910.
- Yan CG, Craddock RC, He Y, Milham MP. 2013. Addressing head motion dependencies for small-world topologies in functional connectomics. *Front Hum Neurosci.* 7:910.
- Yan C-G, Zang Y-F. 2010. DPARSF: a MATLAB toolbox for “pipeline” data analysis of resting-state fMRI. *Front Syst Neurosci.* 4:13.
- Yu Q, Ouyang A, Chalak L, Jeon T, Chia J, Mishra V, Sivarajan M, Jackson G, Rollins N, Liu S, Huang H. 2015. Structural development of human fetal and preterm brain cortical plate based on population-averaged templates. *Cereb Cortex.* 26:4381–4391.
- Zalesky A, Fornito A, Bullmore E. 2012. On the use of correlation as a measure of network connectivity. *Neuroimage.* 60:2096–2106.
- Zuo XN, Ehmke R, Mennes M, Imperati D, Castellanos FX, Sporns O, Milham MP. 2012. Network centrality in the human functional connectome. *Cereb Cortex.* 22:1862–1875.